Explicit versus Parameterized Convection in Response to the Atlantic Meridional Mode

LAURA PACCINI,[a] CATHY HOHENEGGER,[a] AND BJORN STEVENS[a]

[a] *Max Planck Institute for Meteorology, Hamburg, Germany*

(Manuscript received 28 March 2020, in final form 27 October 2020)

ABSTRACT: This study investigates whether the representation of explicit and parameterized convection influences the response to the Atlantic meridional mode (AMM). The main focus is on the precipitation response to the AMM-SST pattern, but possible implications for the atmospheric feedback on SST are also examined by considering differences in the circulation response between explicit and parameterized convection. On the basis of analysis from observations, SST composites are built to represent the positive and negative AMM. These SST patterns, in addition to the March–May climatology, are prescribed to the atmospheric ICON model. High-resolution simulations with explicit convection (E-CON) and coarse-resolution simulations with parameterized convection (P-CON) are used over a nested tropical Atlantic Ocean domain and a global domain, respectively. Our results show that a meridional shift of about 1° in the precipitation climatology explains most of the response to the AMM-SST pattern in simulations both with explicit convection and with parameterized convection. Our results also indicate a linearity in the precipitation response to the positive and negative AMM in E-CON, in contrast to P-CON. Further analysis of the atmospheric response to the AMM reveals that anomalies in the wind-driven enthalpy fluxes are generally stronger in E-CON than in P-CON. This result suggests that SST anomalies would be amplified more strongly in coupled simulations using an explicit representation of convection.

KEYWORDS: Intertropical convergence zone; Atmosphere–ocean interaction; Deep convection

1. Introduction

Convective parameterizations are one of the main simplifications in the representation of atmospheric processes and, despite decades of development, still show difficulties in adequately representing precipitation, particularly in the tropics (e.g., Arakawa 2004; Flato et al. 2014; Fiedler et al. 2020). Over the Atlantic Ocean basin, tropical precipitation is misrepresented both in terms of its intensity and spatial distribution. General circulation models (GCMs) tend to misplace the Atlantic intertropical convergence zone (ITCZ) farther south of its observed position (e.g., Biasutti et al. 2006; Richter and Xie 2008) and to favor precipitation over the east or west Atlantic coast, rather than the central Atlantic as it is observed in the annual mean (Siongco et al. 2015). Biases such as these call into question the representation of the coupling of convection to its environment, particularly SST, with obvious implications for understanding variability and climate change. In this study, we investigate whether the representation of convection influences the response of precipitation to changes in SST.

Over the tropical Atlantic, an important mode of coupled variability is the Atlantic meridional mode (AMM; e.g., Nobre and Shukla 1996; Chiang and Vimont 2004; Xie and Carton 2004). A positive AMM displays warmer than normal SSTs north of the equator, up to 30°N, and cooler than normal south of the equator. Opposite features occur during the negative AMM phase. This interhemispheric difference in SST changes the boundary layer pressure gradient (Lindzen and Nigam 1987), which drives anomalous cross-equatorial surface winds toward the warmer hemisphere (e.g., Chiang and Vimont 2004). As a consequence of the anomalous SST gradient and cross-equatorial winds, the ITCZ is meridionally displaced (e.g., Chiang et al. 2002; Chiang and Vimont 2004). This change in the precipitation pattern also affects the neighboring continents. For instance, positive AMM events are related to dry spells in Northeast Brazil and to wet periods in the northern Amazon and West Africa (e.g., Nobre and Shukla 1996). The precipitation response over land, nevertheless, is not a sole response to the AMM but a result of the combined effect with other modes of variability such as ENSO (e.g., Giannini et al. 2004; Lucena et al. 2011). In contrast, the shift of the ITCZ in the Atlantic basin is the local atmospheric response to AMM-like SST perturbations (Chang et al. 2000; Wang and Carton 2003; Chiang and Vimont 2004) and can be considered the main response to the AMM.

Ocean–atmosphere interactions also play an important role in the AMM development. Positive SST anomalies in the north tropical Atlantic (i.e., positive AMM) are related to weakened trade winds north of the equator. This change in the surface winds suppresses evaporative heat loss, thus favoring a warming of the sea surface. Conversely, negative SST anomalies are related to a strengthening of the surface winds, which leads to surface cooling. This positive feedback, known as the wind–evaporation–SST (WES) feedback (Xie and Philander 1994), has been recognized as a driving mechanism of the AMM (e.g., Amaya et al. 2017). The WES feedback is most pronounced in the northwestern tropical Atlantic and it is stronger during boreal spring when the AMM is more prominent (e.g., Chang et al. 2001; Chiang et al. 2002; Hu and Huang 2006; Foltz et al. 2012; Amaya et al. 2017).

Current GCMs do not represent correctly the coupled SST–precipitation variability in the AMM, since they struggle to reproduce its main driving mechanisms (e.g., Amaya et al. 2017) and do not show a robust atmospheric response to the AMM. Even in atmosphere-only models, the precipitation response to the AMM is far from unanimous. For instance,

Corresponding author: Laura Paccini, laura.paccini@mpimet.mpg.de

DOI: 10.1175/JCLI-D-20-0224.1

Wang and Carton (2003) evaluated the atmospheric response to modes of variability in the tropical Atlantic using a set of uncoupled simulations from various GCMs. They found that only two out of six models represented precipitation and wind anomalies as large as those in observations in response to the AMM mode. Past modeling studies, however, have not evaluated other aspects of the response to the AMM such as the ITCZ displacement.

The inconsistent precipitation response among GCMs may be explained by the different representations of convection and what this implies for their coupling to SST perturbations. In general, parameterized convection is overly sensitive to the surface temperature (e.g., Hirota et al. 2011; Oueslati and Bellon 2015; Siongco et al. 2017) as evidenced by a tendency of GCMs to collocate high precipitation over high SST (Biasutti et al. 2006) to a degree that is not seen in observations. Since convection schemes fail to robustly represent changes in precipitation in response to tropical SST perturbations, it becomes relevant to explore this matter with models that do not parameterize convection. Fortunately, advances in computing allow the use of simulations with explicit convection integrated at convection-permitting resolution of a few kilometers on large domains (Holloway et al. 2012; Marsham et al. 2013; Klocke et al. 2017; Satoh et al. 2019; Stevens et al. 2019). However, the influence of explicit convection in response to SST modes of variability remains unexplored.

In this study, we use both uncoupled convection-permitting simulations as well as coarser-resolution simulations with parameterized convection over the tropical Atlantic and neighboring continents. This allows us to study how precipitation and associated circulation respond to AMM-SST patterns. We assess this coupling from two directions: first the atmospheric response and then its potential feedback on SST. In this latter case, we examine whether differences between explicit and parameterized convection in the surface winds response to the AMM could suggest a distinct change in SST via changes in the magnitude of the surface enthalpy flux, something that would have implications for the representation of modes of variability in the tropics.

This paper is organized as follows. Section 2 is divided into observations and model simulations. First, we present data from observations that are then used to analyze AMM events. This analysis is necessary to determine the SST patterns representative of the AMM that will serve the experimental design. Second, we introduce the model and describe the experimental setup. In section 3, we discuss the main features of the precipitation distribution represented by explicit and parameterized convection, as well as the response to the AMM patterns. Section 4 further explores the possible implications of the atmospheric response, in particular, wind-driven surface fluxes, for changes in SST through the WES feedback. A summary and conclusions are given in section 5.

2. Data and methods

a. Observations

1) Data

For the observational analysis of the AMM mode we study the 1950–2013 period. We use monthly SST data from the Hadley Centre Sea Ice and Sea Surface Temperature dataset (HadISST; Rayner et al. 2003), which is provided on a 1° spatial resolution. Surface winds at 10 m are taken from the National Centers for Environmental Prediction–National Center for Atmospheric Research (NCEP–NCAR) reanalysis dataset (Kalnay et al. 1996) and have a 2.5° spatial grid. Further analysis of the precipitation response to the AMM in observations is performed with data from the Global Precipitation Climatology Project (GPCP; Adler et al. 2003) for the period 1979–2013 at a grid spacing of 2.5°. In addition, we use the TRMM-3B42 V7 rainfall product from the Tropical Rainfall Measuring Mission (Huffman et al. 2007) on a 0.25° spatial grid.

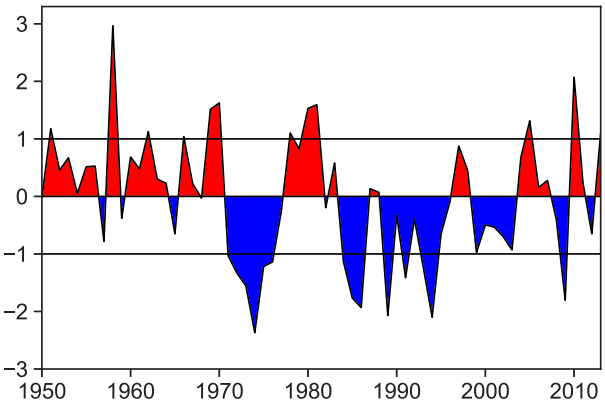

FIG. 1. Seasonal mean of the normalized AMM–SST index for the March–May (MAM) season, based on the index proposed by Chiang and Vimont (2004). Red shaded areas refer to positive AMM, and blue shaded areas refer to negative AMM. The black lines indicate the threshold for the strong AMM events.

To identify AMM events, we use the AMM-SST index proposed by Chiang and Vimont (2004), which is based on NCEP–NCAR reanalysis data. According to their approach, a maximum covariance analysis (MCA) is applied to SST and 10-m wind anomalies over the tropical Atlantic (21°S–32°N, 74°W–15°E). The time series of the AMM index is then constructed by projecting the spatial pattern of the leading MCA mode onto the SST. This study focuses on the March–May (MAM) season (Fig. 1), because it is the time when the AMM signal is strongest (e.g., Chiang and Vimont 2004; Amaya et al. 2017).

2) Building AMM composites

Because of limited computational resources, we are unable to simulate the whole 64-yr period for this study and hence need to build composites of SST patterns representative for positive and negative AMM phases. Since the AMM displays interannual variability with positive and negative events at different intensities (Fig. 1), we build composites that are based on strong events in an effort to better capture the recurrent features of the AMM. The latter are defined by a threshold of 1 unit in the normalized AMM index, equivalent to 1 standard deviation of the time series (Fig. 1). Strong events are defined as those whose seasonal mean index exceeds this threshold. We

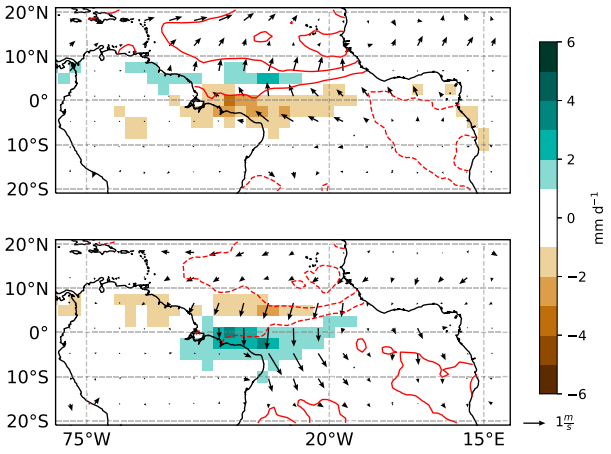

FIG. 2. (top) Positive and (bottom) negative composites of strong AMM events based on SST data for the 1950–2013 SST period. Precipitation anomalies (shaded) are from the GPCP dataset (1979–2013); SST anomalies (positive = solid red line, and negative = red dashed line; intervals each 0.3 K starting at 0.2 K) are from HadISST, and surface wind anomalies (vectors) are from NCEP reanalysis. The 20°W longitude separates the western and eastern Atlantic basins.

then construct from these a composite of strong negative (12 events) and positive (14 events) AMM.

Figure 2 shows the spatial pattern of the AMM composites. In addition to precipitation and SST anomalies, surface wind anomalies are also shown, since the AMM is strongly related to the cross-equatorial winds response (e.g., Nobre and Shukla 1996; Chiang et al. 2002). The SST pattern depicts an antisymmetric dipole with stronger anomalies (up to 0.8 K) over the north tropical Atlantic near the West Africa coast around 10°N. In the Southern Hemisphere, a maximum anomaly of 0.5 K is observed around 10°S. The cross-equatorial wind anomalies are associated with a shift of the mean precipitation that expresses itself as a positive anomaly from about 4° to 10°N for the case of a positive AMM and a negative anomaly for the case of a negative AMM. Over land, the dipole precipitation anomalies are visible along the coast of South America, but details are hard to notice because of the coarse (2.5°) grid spacing. The shift of precipitation is more evident over west of 20°W in the tropical Atlantic. Analysis of individual events show much more variability east of 20°W, which is why significant precipitation anomalies in the eastern basin are hardly visible. On account of these characteristics, we separate the Atlantic basin into a west (75°–20°W) and an east (20°W–15°E) basin for later analysis. The comparison between positive and negative AMM composites show overall opposite symmetric characteristics. The pattern correlation of both AMM composites for SST and precipitation anomalies are −0.95 and −0.88, respectively.

Even though the composites seem to display the expected features associated with AMM events as found in previous studies (e.g., Chiang and Vimont 2004), we further assess their representativeness as compared to specific years. To do this, we compute the pattern correlation of SST and precipitation anomalies among single events (Fig. 3). Here, we only consider the common period with the available precipitation data (1979–2013). The resulting correlation heat maps are arranged according to the AMM index from the greatest (top and left side) to the lowest (bottom and right side) values. The SST patterns are highly correlated within the stronger AMM events (darker colors over the heat-map corners). Likewise, in the case of precipitation, correlation among strong events is greater than among those events with an AMM index between −0.5 and +0.5. In general, the correlation values for precipitation are lower than that for SSTs. This could be due to more variability in precipitation, especially over land. Nonetheless, the highest correlation among the AMM events are within the so-defined strong events for both SST and precipitation. The built composites, thus, illustrate well the main patterns of positive and negative AMM.

b. *Simulations*

1) MODEL

Simulations are performed with the Icosahedral Nonhydrostatic (ICON) model (Zängl et al. 2015) in the numerical weather prediction (NWP) configuration, version 2.3.03. Physical parameterizations are as described in Klocke et al. (2017) and Hohenegger et al. (2020) except that, depending on the grid spacing (see next section), we switch on the parameterization of convection. Convection is parameterized using a bulk mass-flux scheme, which is an implementation based on the Bechtold (2017) modifications to the Tiedtke (1989) convection scheme.

Simulations are initialized from the operational analyses from the European Centre for Medium-Range Weather Forecasts (ECMWF) and Integrated Forecast System (IFS) except for SST, which is taken from the HadISST dataset. We use the ICON tools 2.3.1 for remapping the IFS and HadISST data onto the model grid. Grids and external parameters (like orography and land properties) are obtained via the Online Grid Generator tool provided by the German Meteorological Service (DWD).

2) EXPERIMENTAL SETUP

We conduct the simulations using two representations of moist convection. In the first case, convection is parameterized, and the simulation is referred to as P-CON. P-CON is run over the global domain with a horizontal grid spacing of about 40 km and 90 vertical levels, with the model top at 75 km. In the second configuration the convection scheme is turned off at a convection-permitting resolution, allowing the model to explicitly resolve convection. This simulation is called E-CON. Because of the computational cost, we were unable to perform high-resolution explicit convection simulations at a global scale. Instead, we performed a one-way nesting approach where the P-CON 40-km global simulation provides boundary conditions to nested E-CON domains. Three E-CON nests are applied in which only the horizontal grid spacing is successively stepwise refined from 20 to 10 km and to 5 km over the tropical Atlantic. The refined domains bound the regions 95°W–35°E, 35°S–35°N; 90°W–30°E, 30°S–30°N; and 85°W–25°E, 25°S–25°N,

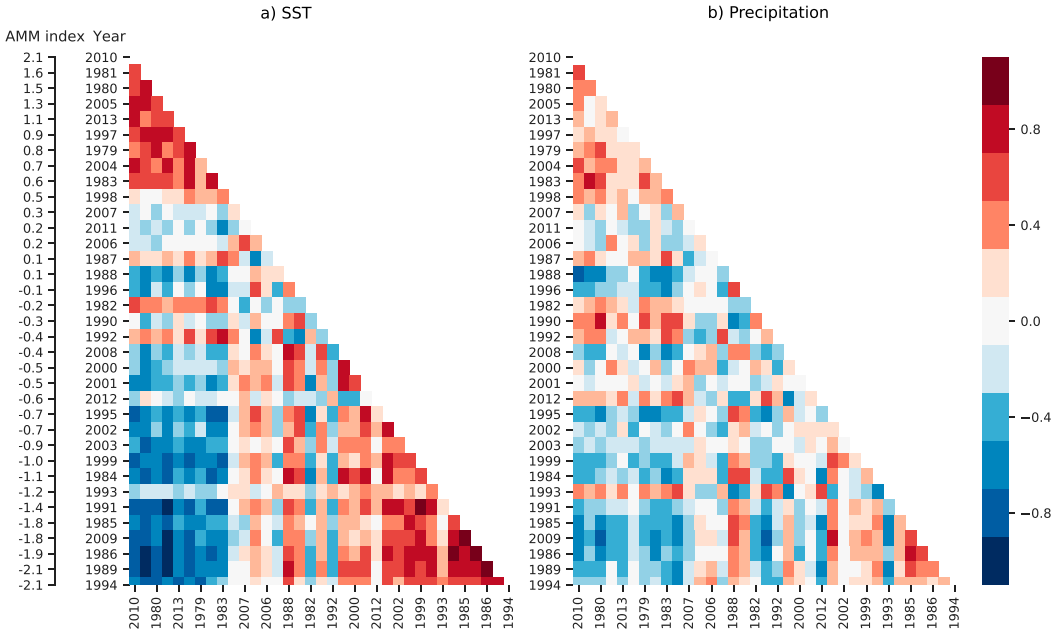

FIG. 3. Correlation heat maps of (a) SST and (b) precipitation anomalies for the 1979–2013 common period. The years are ordered from the greatest value of the AMM index to the lowest value.

respectively. Because of the different grid spacing, the model dynamic time step varies from 360 to 45 s. Time-stepping in the physical parameterizations, such as the cloud-cover time interval, is set to 1080 s in the coarsest resolution and to 900 s for the finest resolution.

To address the concern that the nesting approach might unduly constrain the results, we performed additional simulations using a 20-km grid spacing. The simulations showed no significant difference in terms of overall ITCZ structure, resulting ITCZ shift, and wind response between a global 20-km E-CON and a nested 20-km E-CON simulation. Hence, we find no evidence that the use of a limited domain can spuriously impact the results, at least for the investigated aspects.

In total 12 simulations are performed. P-CON and E-CON start with the same initial conditions and afterward, boundary conditions in E-CON are forced by the P-CON simulation that used the same SST pattern. For each configuration of convection we conduct a pair of simulations for three cases as shown in Table 1. For the control experiments, the MAM SST climatology from 1950 to 2013 is prescribed in the simulations. For the AMM experiments, we imposed the SST patterns from the positive and the negative AMM composites (see previous section). In every case the applied SST is held constant in time. The simulation pairs differ only in their start dates: one is started with the ECMWF–IFS initial conditions of 0000 UTC 27 February 2017, and the other one is started with the initial conditions of 0000 UTC 1 March 2017. The simulation pairs are used to help to assess the influence of internal variability on the results, where each pair of E-CON simulations is driven by its respective P-CON simulation. Simulations are integrated for three months in stand-alone mode. The analysis is performed for the period between 11 March and 31 May, thus allowing 10 days for the simulations to spin up.

3. Sensitivity of precipitation to imposed SST

a. Mean state

We examine the main features of the precipitation as simulated using the climatological SST (control experiments). The mean precipitation amount is 3.5 mm day^{-1} for E-CON and 3.6 mm day^{-1} for P-CON over the 20°S–20°N, 75°W–15°E domain. Values are also similar when only land is considered (3.8

TABLE 1. List of the main characteristics of the experiments (TA = tropical Atlantic).

Expt	SST condition	Convection	Domain	Spatial resolution
E-CON (Clim)	Climatology SST	Explicit	Nested TA	5 km
P-CON (Clim)		Parameterized	Global	40 km
E-CON (+AMM)	Positive AMM SST	Explicit	Nested TA	5 km
P-CON (+AMM)		Parameterized	Global	40 km
E-CON (−AMM)	Negative AMM SST	Explicit	Nested TA	5 km
P-CON (−AMM)		Parameterized	Global	40 km

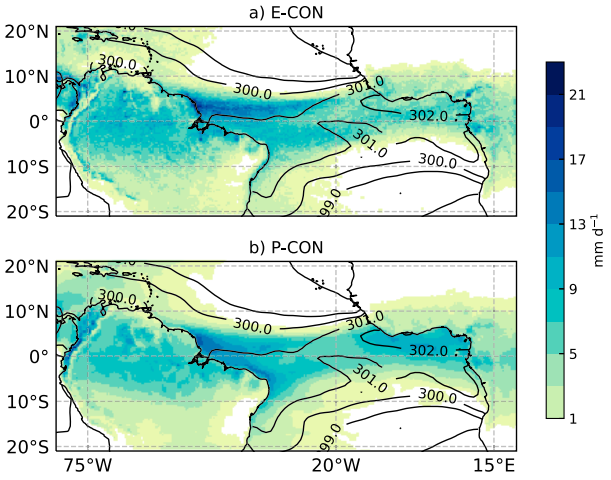

FIG. 4. Mean precipitation (shaded) and prescribed SST climatology (contours) of the 3-month run for (a) E-CON and (b) P-CON simulations interpolated onto the coarser grid of P-CON.

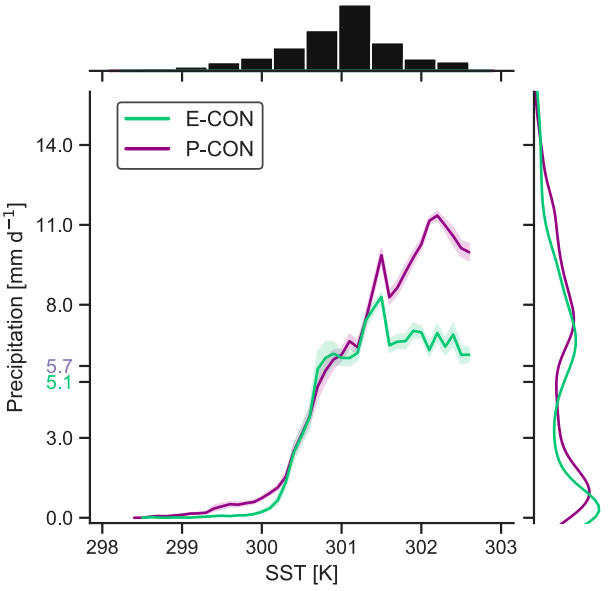

FIG. 5. Average precipitation associated with SST over the deep tropical Atlantic (10°S–10°N, 75°W–15°E). Bins of 0.1 K are used for SST. Mean values of precipitation over the ocean area are highlighted for E-CON (green) and P-CON (purple) simulations. The shaded areas denote the 95% confidence intervals of the simulated values. The histogram of SST and kernel density estimate of precipitation are displayed on the top and right side of the plot, respectively.

and 3.6 mm day^{-1}, respectively). Differences are more marked over the ocean: 2.9 mm day^{-1} for E-CON and 3.4 mm day^{-1} for P-CON. For this reason and because we are interested in the implications for SST coupling, further analysis is focused on this region.

As shown in Fig. 4, both the simulations with parameterized (P-CON) and explicit (E-CON) convection display a double precipitation band that is more pronounced over the west basin. The main difference between E-CON and P-CON, however, is that the precipitation features in P-CON are confined closer to the neighboring continents. E-CON simulates a more zonally elongated distribution, with both bands expanding up to about 15°W, but precipitation maximizing north of the equator (Fig. 4a). The northern band reaches a maximum at about 3°N, whereas the southern band peaks near 4°S. For P-CON, precipitation bands are not as zonally extensive and stay confined westward of 20°W (Fig. 4b). Both bands (north and south) show high precipitation amounts over the eastern coast of South America at about 3°N and 6°S, respectively. Additionally, P-CON displays a second peak of precipitation over the Gulf of Guinea, which is absent in E-CON. Such distinct features of E-CON and P-CON are mostly an effect of the representation of convection, since they persist when coarsening the grid spacing of E-CON to the resolution of P-CON. Moreover, the fact that the main precipitation band extends toward the central basin, in principle, is closer to observations in E-CON than in P-CON. However, one has to be careful to not overinterpret this comparison because our simulations are based on fixed SST composites rather than changing observed SST.

By plotting the precipitation versus SST over the ocean, it becomes apparent that the coastal confinement of precipitation over the Gulf of Guinea in the P-CON simulations is likely the result of P-CON having a stronger sensitivity to SST. Figure 5 shows this clearly, as the precipitation associated with SSTs larger than 301.5 K is much greater for P-CON than it is for E-CON. This is consistent with the predisposition of GCMs relying on convective parameterizations to favor convection over the local SST maximum (Biasutti et al. 2006). Coarsening the grid spacing of E-CON to that of P-CON also leads to an overestimation of precipitation at high SST. This is expected since, by coarsening the grid spacing, the triggering of convection becomes more difficult, which favors convection over high SST regions. Moreover, the well-known pick-up of precipitation with SST is more evident in E-CON at about 300 K. For P-CON, precipitation increases more gradually beginning already at 299 K. This results in a larger area of light precipitation (<3 mm day^{-1}) in the case of P-CON (Fig. 4b and right side in Fig. 5), which is an expression of the well-known drizzle problem of convective parameterizations (Dai 2006).

b. *Response to the AMM-SST pattern*

Figure 6 shows the precipitation, surface wind, and SST anomalies relative to the control experiments for the cases with positive (Figs. 6a,d) and negative (Figs. 6b,e) AMM-SST patterns. In addition, the zonal mean precipitation over the west basin (Figs. 6c,f) is displayed because the observations indicate that in this region the precipitation response is more robust (Fig. 2).

In the case of positive AMM, both E-CON and P-CON display a similar response. This response can be described as an increase of precipitation north of the climatological precipitation bands and a decrease south of them (Figs. 6a,d). This precipitation pattern can be interpreted as resulting from a

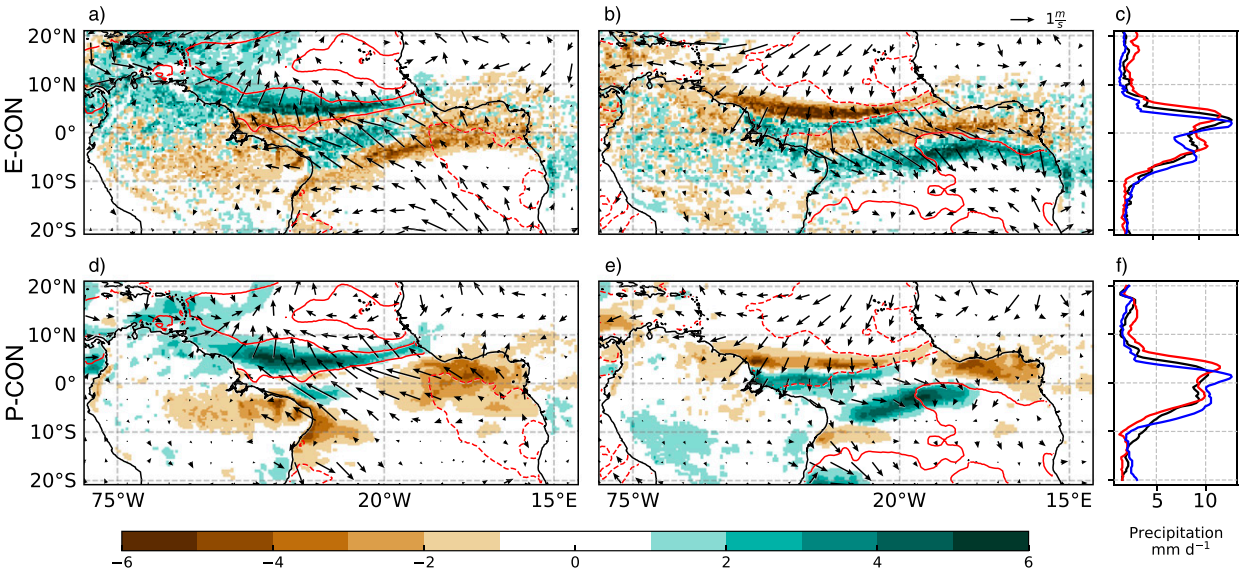

FIG. 6. Precipitation (shaded), SST (contours, with intervals each 0.3 K starting at 0.2 K), and surface wind anomalies (vectors) related to the (a),(d) positive and (b),(e) negative AMM for (top) E-CON and (bottom) P-CON ensemble simulations. The zonal mean precipitation greater than 1 mm day^{-1} over the west Atlantic (75°–20°W) is displayed for (c) E-CON and (f) P-CON. This threshold is chosen to emphasize regions with larger differences. Solid contours refer to the climatology (black contour), positive (red contour), and negative (blue contour) AMM.

northward shift of the climatology. The displacement of the northern precipitation band is apparent for both E-CON and P-CON, whereas the southern band shift is more distinctive in E-CON because of a more prominent double band structure in its precipitation climatology. With respect to land precipitation, the two simulations also exhibit similarities with the positive AMM being associated with a north–south precipitation anomaly. This feature is mainly visible in tropical South America and less so over West Africa in agreement with observations, which do not show a robust precipitation response over land in the eastern basin.

The similarity between E-CON and P-CON over the tropical Atlantic and the apparent shift of the precipitation climatology remains true for the negative AMM experiments (Figs. 6b,e). E-CON and P-CON simulations display enhanced precipitation south of the location of each climatological precipitation band, whereas precipitation decreases toward the north (Figs. 6c,f). The precipitation response over land is less consistent. E-CON depicts a north–south precipitation anomaly over tropical South America between 10°S and 10°N, whereas P-CON displays mostly negative anomalies between 0° and 10°N.

Not only the precipitation response in E-CON and P-CON seems similar, but also the wind pattern response. A cross-equatorial wind flow from 5°S to 5°N in the western Atlantic coincides in both simulations. This picture of precipitation and wind anomalies agrees with observations (Fig. 2). The imprinting of SSTs on boundary layer temperatures, and hence pressure gradients, would drive the surface wind anomalies. The resulting cross-equatorial winds can then be interpreted as driving the meridional shift of the precipitation, as suggested by previous studies (e.g., Hastenrath and Greischar 1993; Chiang et al. 2002; Chiang and Vimont 2004). This interpretation is also consistent with our simulations.

Even though the overall pattern of the oceanic precipitation response to the AMM is similar between E-CON and P-CON, a more detailed look at Fig. 6 also reveals localized discrepancies. These are most notable in the west basin. The zonal mean precipitation of P-CON (Fig. 6f) shows changes in the precipitation intensity in addition to the shift. In particular, the maximum precipitation in P-CON (placed between 0° and 5°N) increases with respect to the climatology in both positive and negative AMM cases. For E-CON (Fig. 6c), changes in the maximum precipitation intensity are less clear than in P-CON. Furthermore, the precipitation amounts over the whole tropical Atlantic basin are about the same for the climatology and AMM (positive and negative) simulations, both in E-CON and P-CON. Therefore, the changes in intensity are localized over the rainiest regions, most notably so for P-CON as compared to E-CON.

A second difference between E-CON and P-CON response to the AMM is apparent when comparing the positive and negative AMM responses. In the case of E-CON, the precipitation responses to the positive and negative AMM are opposite of one another (Figs. 6a,b), which, given the symmetry between positive and negative AMM-SST patterns (Fig. 3a), is indicative of a linear response of precipitation to SST. In contrast, with P-CON the response is less symmetric, most notably so in the southern precipitation band (Figs. 6d,e). In the positive AMM, P-CON keeps the southern band position closer to the South America coast as shown in the climatology (Fig. 4b). In the negative AMM, the southern precipitation

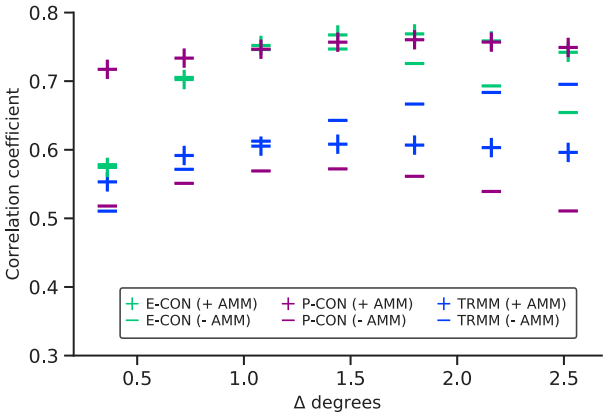

FIG. 7. Correlation of precipitation anomaly maps obtained from shifting the climatology by different degrees in latitude for E-CON (green), P-CON (purple), and observations (TRMM; blue). All data have been interpolated onto the coarser grid of P-CON. Plus and minus symbols indicate the positive and negative AMM cases, respectively.

band of P-CON, extends farther east up to 5°W (not shown). This ''asymmetric'' response to the AMM could be related to the variability of P-CON response. Especially over the south tropical Atlantic, P-CON displayed more inconsistency in the precipitation response among individual simulation members (for all climatology and AMM experiments) in contrast to E-CON, which showed a robust response across all six individual runs (not shown).

c. *Shift in the climatology*

In section 3b, both E-CON and P-CON simulations appeared to predominantly respond to a positive or negative AMM phase by shifting their mean precipitation northward or southward, respectively. This response is consistent with the cross-equatorial winds induced by the interhemispheric difference in SST. The SST pattern, however, is not a result of a meridional displacement in the mean state. Instead, the SST anomalies display an asymmetric pattern that favor the Northern Hemisphere (Fig. 2). In this section, we explore how much of the response can indeed be interpreted simply as a shift of the observed precipitation climatology, with a main focus on the oceanic ITCZ where the shift is more apparent (both in observations and simulations).

For this purpose, the mean precipitation over the ocean between 10°S and 10°N from the control runs is displaced meridionally in proportion to the grid size (0.36°). Then, the precipitation anomalies obtained from shifting the climatology are compared with those from the AMM runs. A similar procedure is applied to precipitation composites from observations, which were interpolated to the model resolution. The results show that interpreting the precipitation response to the AMM as an approximately 1° shift in the precipitation climatology explains a large amount of the precipitation response, with pattern correlations r that are larger than 0.55 for all of the simulations and the observations (Fig. 7). This interpretation works best for E-CON simulations, which depict a correlation of about 0.75 in both positive and negative AMM. For P-CON simulation, a meridional shift in the climatology explains the response of precipitation to the positive AMM ($r = 0.75$) much better than the response to the negative AMM ($r = 0.55$). Given the known biases of convective parameterizations (Fiedler et al. 2020) and the obvious differences in the precipitation climatology between E-CON and P-CON, it is remarkable that the two simulations exhibit an identical shift of 1°. In the case of observations, most of the precipitation response is also explained by the meridional shift of its climatological position. The maximum correlation is 0.6 for positive AMM and about 0.7 for negative AMM. Moreover, the pattern correlation reflects a symmetry in the response for positive and negative AMM at about 1° shift, as it is observed in E-CON.

The analysis of the pattern correlation also highlights the linearity in the meridional shift of precipitation climatology for positive and negative AMM. This is again evident for E-CON and not for P-CON. As explained in the previous section, P-CON displayed an anomalous eastward extension of the southern precipitation band in the negative AMM. This additional change in the precipitation pattern explains the lower correlation obtained in P-CON for the negative AMM ($r = 0.55$). In fact, if the pattern correlation is only computed over western basin, a correlation of 0.75 is obtained as in the positive AMM.

To get a more detailed view on the approach of interpreting the precipitation response as a shift, Fig. 8 shows the precipitation anomalies due to the AMM (shaded) and those obtained from displacing the climatology (contour line) by 1.08°. Overall, there is a very good agreement between the shifted precipitation climatology and the actual response to the AMM for both simulations and observations. This agreement is more apparent in E-CON (Figs. 8a,b), and to a lesser degree in observations (Figs. 8e,f), for both positive and negative AMM. In the case of P-CON (Figs. 8c,d), a shift of the mean precipitation matches the actual precipitation response to the positive and negative AMM principally over the northern basin. South and near the equator discrepancies are more evident. However, as explained in the previous section, P-CON displayed a nonrobust precipitation response in the southern Atlantic when comparing across individual members.

4. Implications for ocean–atmosphere coupling

In the previous section, we explored how the representation of moist convection influences the precipitation response to positive and negative AMM-SST patterns. This addresses the AMM coupled system from one direction. In this section, we examine whether the atmospheric response to the AMM in explicit versus parameterized convection is indicative of a different coupling to the SSTs. This could happen either via a distinct response of the surface fluxes (Vimont 2010; Martinez-Villalobos and Vimont 2016; Amaya et al. 2017) and/or of the radiative fluxes (Evan et al. 2013; Myers et al. 2018), as both control the surface energy budget. Hohenegger et al. (2020) showed that the surface fluxes are robust to changes in grid spacing, whereas the surface radiation (because of its link to low-level cloudiness) is not. Hence, in the following, we focus our analysis on the response of the surface fluxes and how their

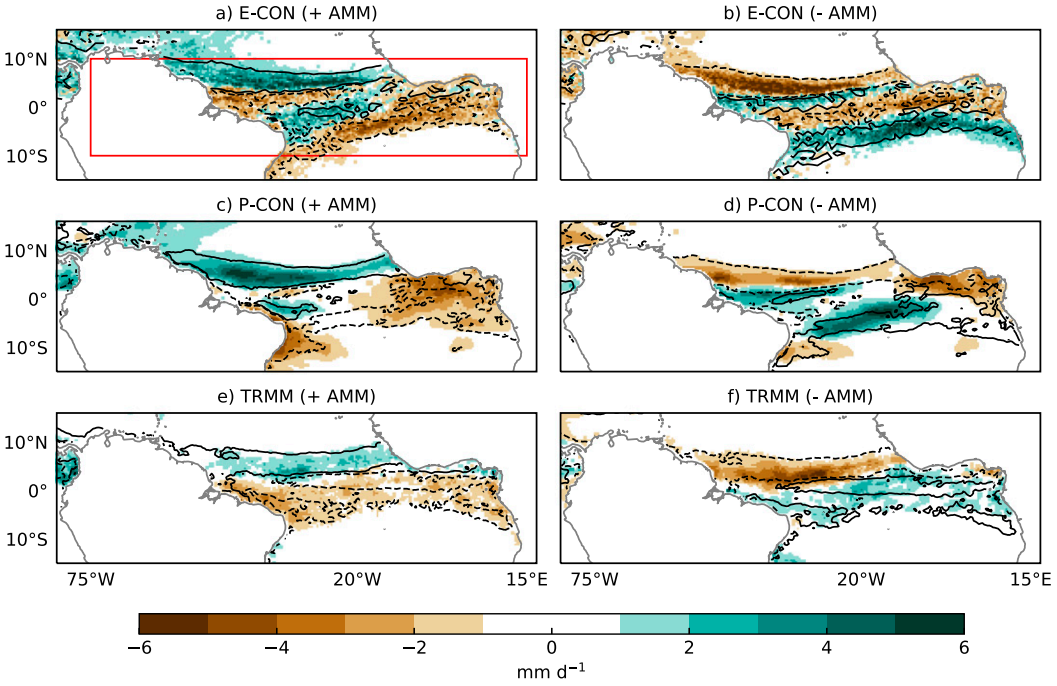

FIG. 8. AMM precipitation anomalies from (a),(b) E-CON, (c),(d) P-CON, and (e),(f) observations (shaded). The resulting anomalies from shifting the climatology are displayed as the 1 mm day^{-1} anomaly contour line (positive = solid line; negative = dashed line). The red-outlined box in (a) indicates where in the ocean the correlation in Fig. 7 was computed.

distinct response in E-CON and P-CON might amplify or dampen the SST anomaly if the simulations were coupled.

We start by examining the representation of the mean wind in E-CON and P-CON, as changes in the wind speed will strongly impact the surface fluxes. Surface winds are generally faster in E-CON than P-CON simulations (Fig. 9) regardless of the experiment or the spatial resolution. This difference can be explained by a stronger pressure gradient in E-CON as shown in Fig. 9, demonstrating that the stronger winds are geostrophically balanced. In particular, along 5°N, the edge of the main precipitation band in the control simulations, we observe a collocation of stronger wind speed and stronger meridional pressure gradient in E-CON as compared to P-CON. North of 5°N, the atmosphere is moister in E-CON than in P-CON below 800 hPa, and drier aloft (Fig. 10). This profile in the humidity distribution favors a stronger radiative cooling by longwave radiation in E-CON north of 5°N, consistent with a colder atmosphere, see the maximum temperature anomaly at about 850 hPa north of 5°N in Fig. 10. The resulting difference in the temperature gradient sets the difference in the surface pressure gradient that in turn sets the difference in the surface winds. This mechanism follows that proposed by Naumann et al. (2019), which generalized the arguments of Lindzen and Nigam (1987) to emphasize the importance of radiative cooling in supporting near-surface pressure gradients.

Differences in the mean state wind speed between E-CON and P-CON translate into different wind speed anomalies as a response to the AMM, with larger anomalies in E-CON (0.3–0.8 m s^{-1} greater in E-CON; not shown). Differences in wind speed will project on the surface enthalpy flux, which will influence the SST, given the constraint of the surface energy budget. Since changes in the surface fluxes influenced by air–sea differences (e.g., Δq) are much less than those influenced by the surface winds (not shown), we focus here on the wind-driven surface enthalpy flux difference $\delta F_h = (\delta V/V)F_h$, where F_h is the surface enthalpy flux (sum of latent and sensible heat flux, defined positive upward) and V is the wind speed at 10 m. We interpret δF_h as the change in the surface enthalpy flux due to a given change in wind. If we assume no changes in the radiative fluxes and given our sign convention, then negative values in δF_h would induce an ocean warming.

In a positive AMM case, a negative δF_h would amplify positive SST anomalies in the northern basin (Figs. 11a,c). The E-CON simulation (Fig. 11a) suggests that most of this amplification over the region 0°–15°N, 60°–30°W, which collocates with the prescribed 0.2–0.5-K SST anomaly. P-CON also suggests an amplification of SST over that region, but of weaker amplitude, and damping of the SST anomaly over the northeast basin where the SST anomalies are highest (+0.8 K). Note here that, according to the observed evolution of the AMM, the importance of wind-induced surface fluxes varies from the subtropical regions (in the preceding boreal winter) toward the southwest equator in boreal spring (Chiang and Vimont 2004; Amaya et al. 2017). Especially during the peak season of the AMM (MAM), the southwestern edge of the SST anomalies (0°–10°N, 50°–20°W) is where the WES feedback is most strongly expressed (e.g., Chang et al. 2001; Chiang et al. 2002;

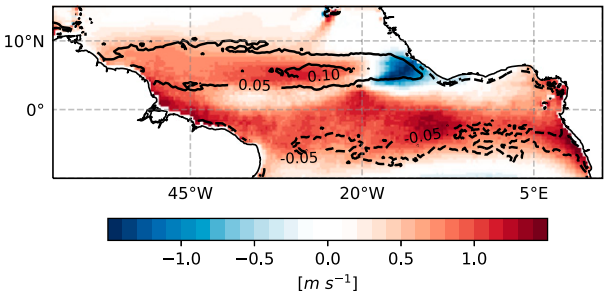

FIG. 9. Surface wind speed (shaded) and meridional pressure gradient (contours; Pa km^{-1}) difference between E-CON and P-CON for the control experiments.

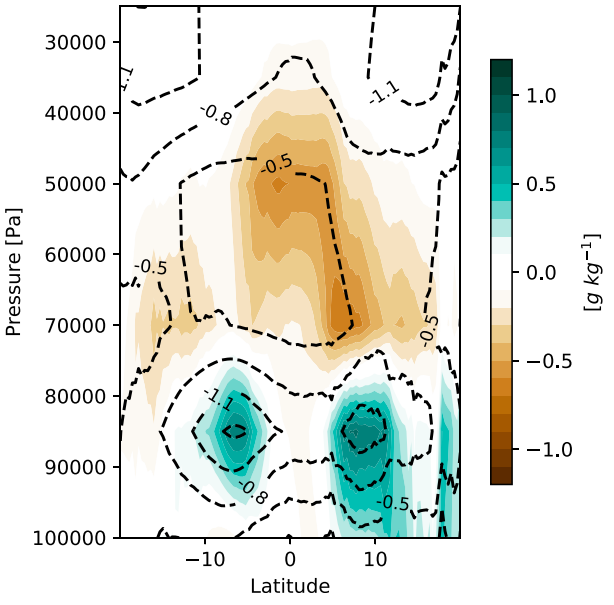

FIG. 10. Meridional cross sections of zonal mean (75°–15°W) specific humidity (shaded) and virtual temperature (contours, with contour interval of 0.3 K) difference between E-CON and P-CON for the control experiments.

Hu and Huang 2006; Foltz et al. 2012; Amaya et al. 2017). It is precisely over this area that stronger δF_h in E-CON is observed as compared to P-CON (Fig. 11e). Moreover, this region is also important for convection to occur, since the northern precipitating bands are placed over those latitudes (Figs. 6a,d). Thus, E-CON not only supports a greater amplification of the SST anomalies, but also sustains convection more strongly than P-CON due to the stronger wind-driven fluxes.

An amplification of the SST anomalies would also be supported in the negative AMM for both E-CON and P-CON (Figs. 11b,d). In this case, the northern basin depicts a broadly positive δF_h, which is indicative of an ocean cooling. However, differences in δF_h between E-CON and P-CON (Fig. 11f) reveal again that E-CON would favor a stronger amplification of the SST anomalies over the northwestern tropical Atlantic (0°–10°N, 50°–20°W).

The abovementioned results suggest that simulations with explicit convection would amplify AMM-SST anomalies more strongly than those with parameterized convection in simulations coupled to an interactive ocean. This would have implications in the representation of the AMM development because the WES feedback is an important driver for sustaining and propagating SST anomalies in the AMM.

5. Summary and conclusions

This study investigates the sensitivity of the coupling between precipitation and SST to the representation of convection, being explicit or parameterized, over the tropical Atlantic. We analyze this coupling in the context of the positive and negative phases of the Atlantic meridional mode (AMM). The AMM is characterized by a warmer than usual north tropical Atlantic and cooler than usual south tropical Atlantic in its positive phase, whereas opposite conditions occur in its negative phase. We focus first on the response of precipitation over ocean to a positive and a negative AMM-SST pattern as compared to the climatology. Then, we investigate possible implications for the coupling to SST.

To fulfil these goals, we use the ICON atmospheric model with the NWP physics configuration. Numerical experiments are performed using SST composites of the climatological, AMM-positive and AMM-negative conditions, respectively. To select the AMM-SST patterns we first examine observations and define "strong" AMM events as those that exceed one standard deviation of the AMM index. Analysis of individual events shows a high degree of similarity among strong AMM events in terms of their SST pattern and associated precipitation response. This analysis supports our methodology approach to build positive and negative AMM composites of strong events. The above mentioned SST patterns are then prescribed to be constant in our simulations integrated from March to May, the season when the AMM is more prominent. Two configurations are applied: one with convective parameterization (P-CON) at a grid spacing of 40 km on a global domain; and one with the convective parameterization turned off (E-CON) at a grid spacing of 5 km over a nested tropical Atlantic domain.

Because of the intensive amount of computation required for the E-CON simulations, they could not be integrated globally like P-CON and only two members were simulated. Such a small number of samples may spuriously affect the results. However, differences between E-CON and P-CON simulations are larger than differences among E-CON and P-CON respective members. In fact, features such as the ITCZ structure, wind speed velocity, and vertical profile of temperature and humidity are consistent regardless of the experiment. Moreover, a global simulation conducted with a grid spacing of 20 km revealed similar results to the 20-km nested simulations. Hence, we believe the framework to be informative, despite the small number of simulations.

On the basis of the analysis of these simulations we address two questions: 1) Does the precipitation response to AMM-SST patterns differ when convection is explicitly resolved as

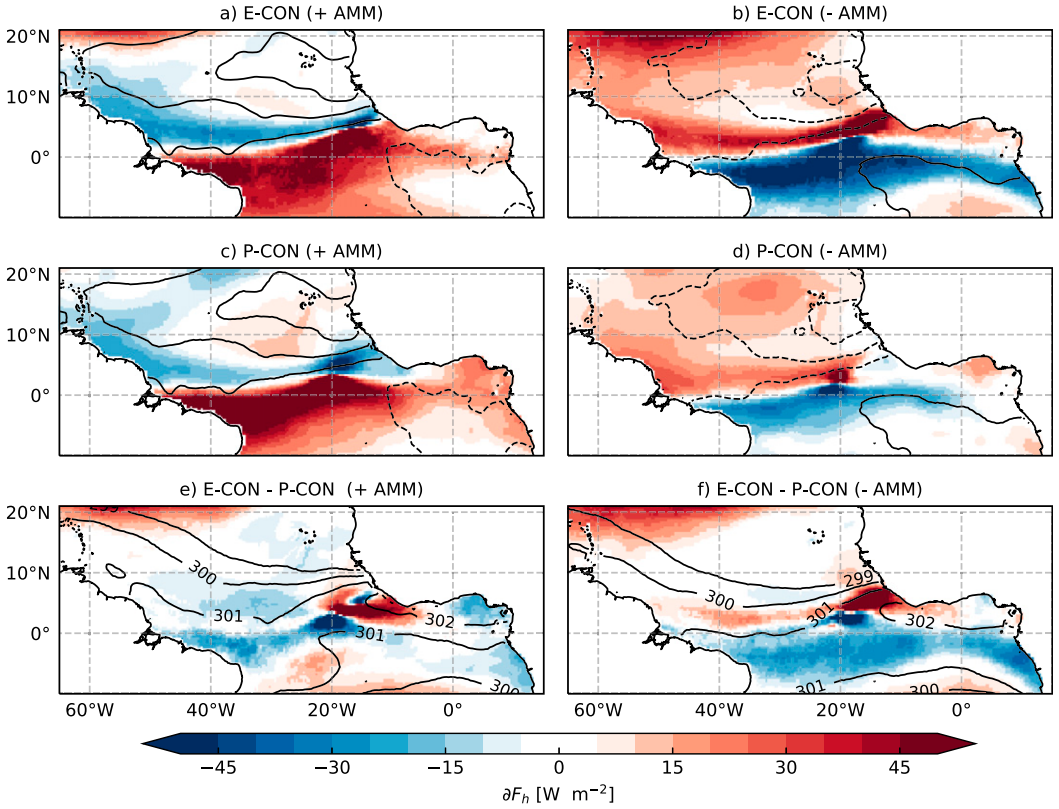

FIG. 11. Wind-driven surface enthalpy flux (shading) for a (left) positive and (right) negative AMM, in (a),(b) E-CON and (c),(d) P-CON simulations. Blue colors denote a reduction of the surface fluxes and suggest an ocean warming, whereas red colors denote an increase of the surface fluxes and suggest an ocean cooling. The plots also show prescribed SST anomalies (contours, with interval of 0.3 K). The difference between E-CON and P-CON simulations is displayed for (e) positive and (f) negative AMM with its corresponding mean SST (contours).

opposed to parameterized convection? 2) Does the atmospheric response in explicit and parameterized convection suggest different couplings to the underlying SSTs?

1) We find that the precipitation response to an AMM-SST pattern is robust to the representation of convection. Simulations with explicit and with parameterized convection show a similar response. Both E-CON and P-CON simulations shift the mean position of the ITCZ about one degree toward the warmer tropical Atlantic. Interestingly, this is true even though E-CON and P-CON display a distinct precipitation climatology: P-CON shows a stronger precipitation sensitivity to high SST than E-CON and thus, places an extra peak of precipitation in the eastern basin, coinciding with the maximum SST. Different precipitation patterns are also displayed in response to the AMM but are the result of shifting the precipitation climatology. The meridional displacement in the precipitation can be explained by the cross-equatorial surface wind anomalies induced by the AMM-SST gradient (e.g., Chiang et al. 2002; Chiang and Vimont 2004), with the precipitation being shifted toward the region where winds weaken. Our results showed that the latitudinal range where the wind anomalies occur (5°S–5°N) is about the same for both simulations, which may explain the similar displacement in the Atlantic ITCZ for E-CON and P-CON.

   Despite this overall similarity in the precipitation response between E-CON and P-CON, some discrepancies can also be noted. In addition to the meridional shift of precipitation, there are localized changes in the precipitation intensity. These changes are more obvious over the rainiest regions in P-CON as compared to E-CON. Furthermore, our results indicate a linearity in the response of E-CON to the AMM. The meridional shift of the mean precipitation explains about 60% ($r = 0.75$) of the precipitation response for both positive and negative AMM in E-CON simulations. In contrast, the precipitation response as explained by the meridional shift in P-CON explains 60% in the positive AMM but only 30% ($r = 0.55$) in the negative AMM. Only over the west tropical Atlantic do we find a symmetry (and hence linearity) in the precipitation shift between positive and negative AMM for P-CON.
2) Analysis of surface flux anomalies lead us to expect a stronger amplification of SST anomalies in simulations with explicit rather than parameterized convection. Our argument is based on the wind speed anomalies in response to an AMM-SST pattern. Surface winds are generally stronger in E-CON

because of a stronger pressure gradient, itself related to stronger radiative cooling north of 5°N, a result of a moister boundary layer and drier free atmosphere. The changes in the wind-driven heat fluxes are, in consequence, more strongly enhanced in E-CON. Positive SST anomalies in the north tropical Atlantic (positive AMM) would be amplified when the change in the wind-driven surface flux is negative. Therefore, a stronger amplification of the SST anomalies would be induced by a stronger enhancement of the wind-driven heat flux in E-CON as compared to P-CON. In particular, stronger wind-driven fluxes in E-CON than P-CON were visible over the region where the wind–evaporation–SST (WES) feedback has been identified by previous studies to play an important role on the development of the AMM (e.g., Amaya et al. 2017). Differences between E-CON and P-CON over this region are mostly evident in the positive AMM case and to a lesser extent in the negative AMM.

From these results, we hypothesize that coupled simulations with explicit convection would lead to stronger amplification of the SST anomalies, affecting the development and propagation of the AMM mode, in comparison with coupled simulations with parameterized convection.

Acknowledgments. This study was supported by the Max Planck Society for the Advancement of Science. The authors thank Traute Crueger and three anonymous reviewers for their useful and constructive comments on the paper.

Data availability statement. The AMM-SST index is provided by the NOAA Earth System Research Laboratory (ESRL) for free (https://www.esrl.noaa.gov/psd/data/timeseries/monthly/AMM/). GPCP precipitation and NCEP reanalysis data are provided by the NOAA/OAR/ESRL PSD (https://www.esrl.noaa.gov/psd/). TRMM data were retrieved via the NASA Goddard Earth Sciences (GES) Data and Information Services Center (http://disc.sci.gsfc.nasa.gov/). Primary data and scripts used in the analysis that may be useful in reproducing the author's work are archived by the Max Planck Institute for Meteorology and can be obtained by contacting publications@mpimet.mpg.de.

REFERENCES

Adler, R. F., and Coauthors, 2003: The version-2 Global Precipitation Climatology Project (GPCP) monthly precipitation analysis (1979–present). *J. Hydrometeor.*, **4**, 1147–1167, https://doi.org/10.1175/1525-7541(2003)004<1147:TVGPCP>2.0.CO;2.

Amaya, D. J., M. J. DeFlorio, A. J. Miller, and S.-P. Xie, 2017: WES feedback and the Atlantic meridional mode: Observations and CMIP5 comparisons. *Climate Dyn.*, **49**, 1665–1679, https://doi.org/10.1007/s00382-016-3411-1.

Arakawa, A., 2004: The cumulus parameterization problem: Past, present, and future. *J. Climate*, **17**, 2493–2525, https://doi.org/10.1175/1520-0442(2004)017<2493:RATCPP>2.0.CO;2.

Bechtold, P., 2017: Atmospheric moist convection. ECMWF Meteorological Training Course Lecture Series Doc., 85 pp., https://www.ecmwf.int/node/16953.

Biasutti, M., A. Sobel, and Y. Kushnir, 2006: AGCM precipitation biases in the tropical Atlantic. *J. Climate*, **19**, 935–958, https://doi.org/10.1175/JCLI3673.1.

Chang, P., R. Saravanan, L. Ji, and G. C. Hegerl, 2000: The effect of local sea surface temperatures on atmospheric circulation over the tropical Atlantic sector. *J. Climate*, **13**, 2195–2216, https://doi.org/10.1175/1520-0442(2000)013<2195:TEOLSS>2.0.CO;2.

——, L. Ji, and R. Saravanan, 2001: A hybrid coupled model study of tropical Atlantic variability. *J. Climate*, **14**, 361–390, https://doi.org/10.1175/1520-0442(2001)013<0361:AHCMSO>2.0.CO;2.

Chiang, J. C., and D. J. Vimont, 2004: Analogous Pacific and Atlantic meridional modes of tropical atmosphere–ocean variability. *J. Climate*, **17**, 4143–4158, https://doi.org/10.1175/JCLI4953.1.

——, Y. Kushnir, and A. Giannini, 2002: Deconstructing Atlantic Intertropical Convergence Zone variability: Influence of the local cross-equatorial sea surface temperature gradient and remote forcing from the eastern equatorial Pacific. *J. Geophys. Res.*, **107**, 4004, https://doi.org/10.1029/2000JD000307.

Dai, A., 2006: Precipitation characteristics in eighteen coupled climate models. *J. Climate*, **19**, 4605–4630, https://doi.org/10.1175/JCLI3884.1.

Evan, A. T., R. J. Allen, R. Bennartz, and D. J. Vimont, 2013: The modification of sea surface temperature anomaly linear damping time scales by stratocumulus clouds. *J. Climate*, **26**, 3619–3630, https://doi.org/10.1175/JCLI-D-12-00370.1.

Fiedler, S., and Coauthors, 2020: Simulated tropical precipitation assessed across three major phases of the Coupled Model Intercomparison Project (CMIP). *Mon. Wea. Rev.*, **148**, 3653–3680, https://doi.org/10.1175/MWR-D-19-0404.1.

Flato, G., and Coauthors, 2014: Evaluation of climate models. *Climate Change 2013: The Physical Science Basis*, T. F. Stocker et al., Eds., Cambridge University Press, 741–866.

Foltz, G. R., M. J. McPhaden, and R. Lumpkin, 2012: A strong Atlantic meridional mode event in 2009: The role of mixed layer dynamics. *J. Climate*, **25**, 363–380, https://doi.org/10.1175/JCLI-D-11-00150.1.

Giannini, A., R. Saravanan, and P. Chang, 2004: The preconditioning role of tropical Atlantic variability in the development of the ENSO teleconnection: Implications for the prediction of Nordeste rainfall. *Climate Dyn.*, **22**, 839–855, https://doi.org/10.1007/s00382-004-0420-2.

Hastenrath, S., and L. Greischar, 1993: Circulation mechanisms related to Northeast Brazil rainfall anomalies. *J. Geophys. Res.*, **98**, 5093–5102, https://doi.org/10.1029/92JD02646.

Hirota, N., Y. N. Takayabu, M. Watanabe, and M. Kimoto, 2011: Precipitation reproducibility over tropical oceans and its relationship to the double ITCZ problem in CMIP3 and MIROC5 climate models. *J. Climate*, **24**, 4859–4873, https://doi.org/10.1175/2011JCLI4156.1.

Hohenegger, C., L. Kornblueh, D. Klocke, T. Becker, G. Cioni, J. F. Engels, U. Schulzweida, and B. Stevens, 2020: Climate statistics in global simulations of the atmosphere, from 80 to 2.5 km grid spacing. *J. Meteor. Soc. Japan*, **98**, 73–91, https://doi.org/10.2151/jmsj.2020-005.

Holloway, C., S. Woolnough, and G. Lister, 2012: Precipitation distributions for explicit versus parametrized convection in a large-domain high-resolution tropical case study. *Quart. J. Roy. Meteor. Soc.*, **138**, 1692–1708, https://doi.org/10.1002/qj.1903.

Hu, Z.-Z., and B. Huang, 2006: Physical processes associated with the tropical Atlantic SST meridional gradient. *J. Climate*, **19**, 5500–5518, https://doi.org/10.1175/JCLI3923.1.

Huffman, G. J., and Coauthors, 2007: The TRMM Multisatellite Precipitation Analysis (TMPA): Quasi-global, multiyear, combined-sensor precipitation estimates at fine scales. *J. Hydrometeor.*, **8**, 38–55, https://doi.org/10.1175/JHM560.1.

Kalnay, E., and Coauthors, 1996: The NCEP/NCAR 40-Year Reanalysis Project. *Bull. Amer. Meteor. Soc.*, **77**, 437–471, https://doi.org/10.1175/1520-0477(1996)077<0437:TNYRP>2.0.CO;2.

Klocke, D., M. Brueck, C. Hohenegger, and B. Stevens, 2017: Rediscovery of the doldrums in storm-resolving simulations over the tropical Atlantic. *Nat. Geosci.*, **10**, 891–896, https://doi.org/10.1038/s41561-017-0005-4.

Lindzen, R. S., and S. Nigam, 1987: On the role of sea surface temperature gradients in forcing low-level winds and convergence in the tropics. *J. Atmos. Sci.*, **44**, 2418–2436, https://doi.org/10.1175/1520-0469(1987)044<2418:OTROSS>2.0.CO;2.

Lucena, D. B., J. Servain, and M. F. Gomes Filho, 2011: Rainfall response in Northeast Brazil from ocean climate variability during the second half of the twentieth century. *J. Climate*, **24**, 6174–6184, https://doi.org/10.1175/2011JCLI4194.1.

Marsham, J. H., N. S. Dixon, L. Garcia-Carreras, G. M. Lister, D. J. Parker, P. Knippertz, and C. E. Birch, 2013: The role of moist convection in the West African monsoon system: Insights from continental-scale convection-permitting simulations. *Geophys. Res. Lett.*, **40**, 1843–1849, https://doi.org/10.1002/grl.50347.

Martinez-Villalobos, C., and D. J. Vimont, 2016: The role of the mean state in meridional mode structure and growth. *J. Climate*, **29**, 3907–3921, https://doi.org/10.1175/JCLI-D-15-0542.1.

Myers, T. A., C. R. Mechoso, and M. J. DeFlorio, 2018: Importance of positive cloud feedback for tropical Atlantic interhemispheric climate variability. *Climate Dyn.*, **51**, 1707–1717, https://doi.org/10.1007/s00382-017-3978-1.

Naumann, A. K., B. Stevens, and C. Hohenegger, 2019: A moist conceptual model for the boundary layer structure and radiatively driven shallow circulations in the trades. *J. Atmos. Sci.*, **76**, 1289–1306, https://doi.org/10.1175/JAS-D-18-0226.1.

Nobre, P., and J. Shukla, 1996: Variations of sea surface temperature, wind stress, and rainfall over the tropical Atlantic and South America. *J. Climate*, **9**, 2464–2479, https://doi.org/10.1175/1520-0442(1996)009<2464:VOSSTW>2.0.CO;2.

Oueslati, B., and G. Bellon, 2015: The double ITCZ bias in CMIP5 models: Interaction between SST, large-scale circulation and precipitation. *Climate Dyn.*, **44**, 585–607, https://doi.org/10.1007/s00382-015-2468-6.

Rayner, N., D. E. Parker, E. Horton, C. K. Folland, L. V. Alexander, D. Rowell, E. Kent, and A. Kaplan, 2003: Global analyses of sea surface temperature, sea ice, and night marine air temperature since the late nineteenth century. *J. Geophys. Res.*, **108**, 4407, https://doi.org/10.1029/2002JD002670.

Richter, I., and S.-P. Xie, 2008: On the origin of equatorial Atlantic biases in coupled general circulation models. *Climate Dyn.*, **31**, 587–598, https://doi.org/10.1007/s00382-008-0364-z.

Satoh, M., B. Stevens, F. Judt, M. Khairoutdinov, S.-J. Lin, W. M. Putman, and P. Düben, 2019: Global cloud-resolving models. *Curr. Climate Change Rep.*, **5**, 172–184, https://doi.org/10.1007/S40641-019-00131-0.

Siongco, A. C., C. Hohenegger, and B. Stevens, 2015: The Atlantic ITCZ bias in CMIP5 models. *Climate Dyn.*, **45**, 1169–1180, https://doi.org/10.1007/s00382-014-2366-3.

——, ——, and ——, 2017: Sensitivity of the summertime tropical Atlantic precipitation distribution to convective parameterization and model resolution in ECHAM6. *J. Geophys. Res. Atmos.*, **122**, 2579–2594, https://doi.org/10.1002/2016JD026093.

Stevens, B., and Coauthors, 2019: DYAMOND: The dynamics of the atmospheric general circulation modeled on non-hydrostatic domains. *Prog. Earth Planet. Sci.*, **6**, 61, https://doi.org/10.1186/s40645-019-0304-z.

Tiedtke, M., 1989: A comprehensive mass flux scheme for cumulus parameterization in large-scale models. *Mon. Wea. Rev.*, **117**, 1779–1800, https://doi.org/10.1175/1520-0493(1989)117<1779:ACMFSF>2.0.CO;2.

Vimont, D. J., 2010: Transient growth of thermodynamically coupled variations in the tropics under an equatorially symmetric mean state. *J. Climate*, **23**, 5771–5789, https://doi.org/10.1175/2010JCLI3532.1.

Wang, J., and J. A. Carton, 2003: Modeling climate variability in the tropical Atlantic atmosphere. *J. Climate*, **16**, 3858–3876, https://doi.org/10.1175/1520-0442(2003)016<3858:MCVITT>2.0.CO;2.

Xie, S.-P., and S. G. H. Philander, 1994: A coupled ocean–atmosphere model of relevance to the ITCZ in the eastern Pacific. *Tellus*, **46A**, 340–350, https://doi.org/10.3402/tellusa.v46i4.15484.

——, and J. A. Carton, 2004: Tropical Atlantic variability: Patterns, mechanisms, and impacts. *Earth Climate: The Ocean–Atmosphere Interaction*, *Geophys. Monogr.*, Vol. 147, Amer. Geophys. Union, 121–142.

Zängl, G., D. Reinert, P. Rípodas, and M. Baldauf, 2015: The ICON (ICOsahedral Non-hydrostatic) modelling framework of DWD and MPI-M: Description of the non-hydrostatic dynamical core. *Quart. J. Roy. Meteor. Soc.*, **141**, 563–579, https://doi.org/10.1002/qj.2378.